

Enhanced the tunable omnidirectional photonic band gaps in the two-dimensional plasma photonic crystals

Hai-Feng Zhang^{1,2} · Shao-Bin Liu²

Received: 17 April 2016 / Accepted: 22 October 2016 / Published online: 26 October 2016
© Springer Science+Business Media New York 2016

Abstract In this paper, the features of omnidirectional band gap (OBG) in the two-dimensional (2D) plasma photonic crystals (PPCs) with triangular lattices are theoretically studied in detail by the modified plane wave expansion method as the off-plane incidence wave vector is considered, which are composed of the non-magnetized plasma cylinders inserted into the homogeneous and isotropic dielectric background. The simulated results demonstrate that a flatband region and the OBG can be obtained in the proposed PPCs. The influences of the radius of inserted cylinder and plasma frequency on the OBG are investigated. The calculated results illustrate that not only the tunable OBG can be obtained but also the achieved OBG also can be enlarged by optimizing those parameters. To enhance the OBGs, two novel configurations of PPCs are present. The computed results reveal that the proposed two configurations have the advantages of obtaining the larger OBGs compared to the conventional 2D PPCs since the symmetry of 2D PPCs is broken, and the OBGs also can be manipulated obviously by changing the geometric parameters of such two PCs structures. Introducing the anisotropic dielectric (uniaxial material) into the proposed 2D PPCs to enlarge the OBGs also is studied. The effects of ordinary-refractive and extraordinary-refractive indices of uniaxial material on the properties of OBGs also are investigated in theory, respectively. The computed results show that the OBGs can be enlarged by introducing the uniaxial material, and the OBGs also can be tuned by changing the parameters of uniaxial material.

Keywords Two-dimensional plasma photonic crystals · Photonic band gap · Complete photonic band gap · Omnidirectional band gap · Plane wave expansion method

✉ Hai-Feng Zhang
hanlor@163.com

¹ School of Optoelectronic Engineering, Nanjing University of Posts and Telecommunications, Nanjing 210023, China

² Key Laboratory of Radar Imaging and Microwave Photonics (Nanjing Univ. Aeronaut. Astronaut.), Ministry of Education, Nanjing University of Aeronautics and Astronautics, Nanjing 210016, China

1 Introduction

Since the existence of photonic band gaps (PBGs) (Joannopoulos et al. 1995), the photonic crystals (PCs) become a attractive research focus after firstly proposed in 1987 (Yablonovitch 1987; John 1987), in which the electromagnetic (EM) waves can be forbidden because of the interference of multiple Bragg scattering (Joannopoulos et al. 1995). It means that the researchers can manipulate the EM waves to propagate in a certain direction or frequency only by arranging the different dielectric materials in space periodically. Thus, many important and valuable practical devices can be realized by the PCs (Mekis et al. 1996; Russell 2003; Biancalana 2008). If two different polarized EM waves (TE and TM waves) are forbidden at same time, the complete PBGs (CPBGs) can be obtained. To the PCs, if the CPBGs can be achieved in any direction, the omnidirectional band gap (OBG) will be obtained. Compared to the PBGs, the OBGs have more practical values, which can be used to design many applications (Xiang et al. 2007; Hart et al. 2002; Winn et al. 1998). However, the OBG is difficult to obtain in the conventional dielectric PCs, whose PBGs also cannot be manipulated and strongly depend on the topology of PCs. To overcome those shortcomings, the dispersive materials or metamaterials are introduced into the conventional PCs to enlarge or obtain the tunable PBGs, such as metal (Chern et al. 2006), semiconductor (Tian and Zi 2005), plasma (Hojo and Mase 2004) and superconductor (Aly et al. 2014). In the nature, the physical features of plasma can be manipulated by many external factors (Sakai and Tachibana 2012; Ginzburg 1970). Thus, the plasma photonic crystals (PPCs) become an good candidate to achieve the tunable CPBGs or OBGs since it was firstly proposed by Hojo et al. (Hojo and Mase 2004) in 2004. Especially, more complicated EM modes and interesting phenomena can be observed in the magnetized PPCs (Qi 2012; King et al. 2013; Zhang et al. 2015c). Thus, the PPCs have attracted tremendous interests of researchers during past 10 years.

As time goes on, the PPCs have been extensively studied in the theory and experiment, especially, for one-dimensional (1D) and 2D cases. The properties of PBGs and defect modes of 1D and 2D PPCs are investigated by many researchers even as the external magnetic field is considered (Qi 2012; King et al. 2013; Zhang et al. 2015a, b; Shiverhwari 2011). In recently, the many interesting phenomena in the PPCs are analyzed in detail such as evanescent wave (Li et al. 2011), surface plasmon modes (Zhang and Liu 2014), surface modes (Shukla et al. 2015) and nonreciprocal propagation (Ardakani 2014). The novel properties for the different ways to form the PPCs also are studied (Fu et al. 2013; Hamidi 2012; Qi and Zhang 2011). However, in those works, the properties of PBGs are focused on the PBGs since the CPBGs are hardly observed in the conventional 1D or 2D PPCs. In other words, not all of PBGs in the 1D and 2D cases are the CPBGs. Thus, the 1D and 2D PPCs have to be redesigned for obtaining CPBGs and OBGs, such as introducing the new filler into 2D case (Zhang et al. 2015c), using heterostructure (Zhang et al. 2013a), introducing matching layer (Zhang et al. 2012a) and arranging aperiodic structure (Zhang et al. 2012b) to the 1D cases. In theory, the 3D PPCs (Joannopoulos et al. 1995; Zhang et al. 2013b) are more suitable to achieve the OBGs compared to the 1D and 2D cases. However, the 3D PPCs have to suffer from fabrication defects or irregularities, and 1D PPCs also have many problems in realizing the devices for its large thickness and finite height system (Li and Xia 2001; Haas et al. 2006). As mentioned by (Li and Xia 2001) and Hass et al. (2006), the so-called 2.5D PCs structure becomes a good choice in obtaining or enlarging the OBGs since the shortcomings appearing in the 1D and 3D cases can be overcome as the EM waves are incident with an off-plane angle. The larger OBG has

potential application in the omnidirectional high reflector, all-dielectric coaxial waveguide, omnidirectional mirror fiber, omnidirectional high-quality filter, antenna substrates. Obviously, in order to obtain the OBG from 2D PPCs, the properties of 2D PPCs with off-plane wave vector has to be investigated.

In this paper, the aims are to investigate the features of OBG in the 2D PPCs with triangular lattices by the plane wave expansion (PWE) method, which are composed of the non-magnetized plasma cylinders inserted into the homogeneous and isotropic dielectric background. We also further study the properties of OBG for the two novel PCs configurations. Breaking the symmetrical profile of PPCs also is a good way to enlarge the OBGs according to the practical applications. Introducing the anisotropic dielectric (uniaxial material) into the 2D PPCs also can enlarge the OBGs. We assume the time-harmonic variable is $e^{-j\omega t}$ (ω is the angular frequency and $j = \sqrt{-1}$), and c is the light speed in vacuum.

2 Theoretical model and numerical method

In Fig. 1, the schematic structure of 2D PPCs and the first irreducible Brillouin zone are plotted. As shown in Fig. 1, we consider the lattice constant and the radius of inserted plasma cylinders are a and R , respectively. We also assume the relative dielectric functions for the dielectric background and plasma cylinders are ϵ_a and ϵ_p , respectively. One also can see from Fig. 1 that the high symmetry points for the first irreducible Brillouin zone are $\Gamma = (0, 0)$, $J = (2\sqrt{3}\pi/3a, 0)$, and $X = (2\sqrt{3}\pi/3a, 2\pi/3a)$ (Li and Xia 2001; Feng and Arakawa 1996). Obviously, the EM wave are obliquely incident into the 2D PPCs with an angle θ , where the angle between the incident wave vector \mathbf{k} and wave vector in the in-plane case is θ . It means that the wave vector \mathbf{k} has a component in z direction, which is $k_z = \omega \sin\theta/c$. As we know, ϵ_p can be expressed as (Ginzburg 1970)

$$\epsilon_p = 1 - \frac{\omega_p^2}{\omega(\omega + j\nu_c)} \tag{1}$$

where ν_c and ω_p are the plasma collision frequency and plasma frequency, respectively. In order to compute the OBGs of proposed 2D PPCs, the modified PWE method is used

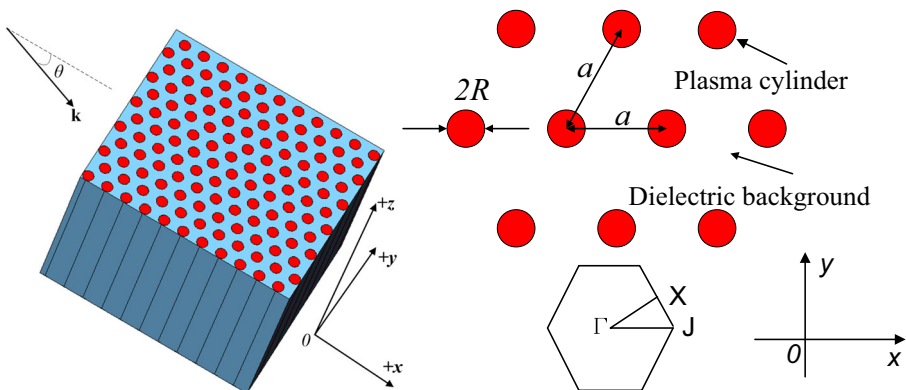


Fig. 1 Schematic structure of such 2D PPCs and the first irreducible Brillouin zone for computing the band structures

(Sakoda 2001; Kuzmiak and Maradudin 1997). The details of how to compute the band structures for the 2D PPCs with off-plane case can be found in the Ref. (Zhang et al. 2016).

3 Numerical results and analysis

In the following calculations, the frequency region is normalized by a constant $\omega_0 = \omega a / 2\pi c$ and the initial values of ω_p and v_c are defined as $\omega_p = 0.2\omega_0$ and $v_c = 0.003\omega_p$, respectively. The 1225 plane waves and 30 k -vector also are utilized to calculate the OBGs to obtain a enough accuracy (Sözüer et al. 1992).

3.1 The properties of OBG in the proposed 2D PPCs

In Fig. 2, we plot the band structures for such PPCs with different incidence angle θ as $\varepsilon_a = 12.96$, $R = 0.46a$, $\omega_p = 0.2\omega_0$ and $v_c = 0.003\omega_p$. The red shaded regions indicate the OBGs. Those dielectric cylinders are GaAs, whose the refractive index is equal to 3.6. It can be seen from Fig. 2 that not only there is an OBG which is located between third and fourth bands above the flatband region, but also one flatband region can be observed. The OBG covers from 0.4830 to 0.5038 ($2\pi c/a$), and the flatband region runs from 0 to 0.2 ($2\pi c/a$). In the flatband region, the group velocity of EM wave is every low since the

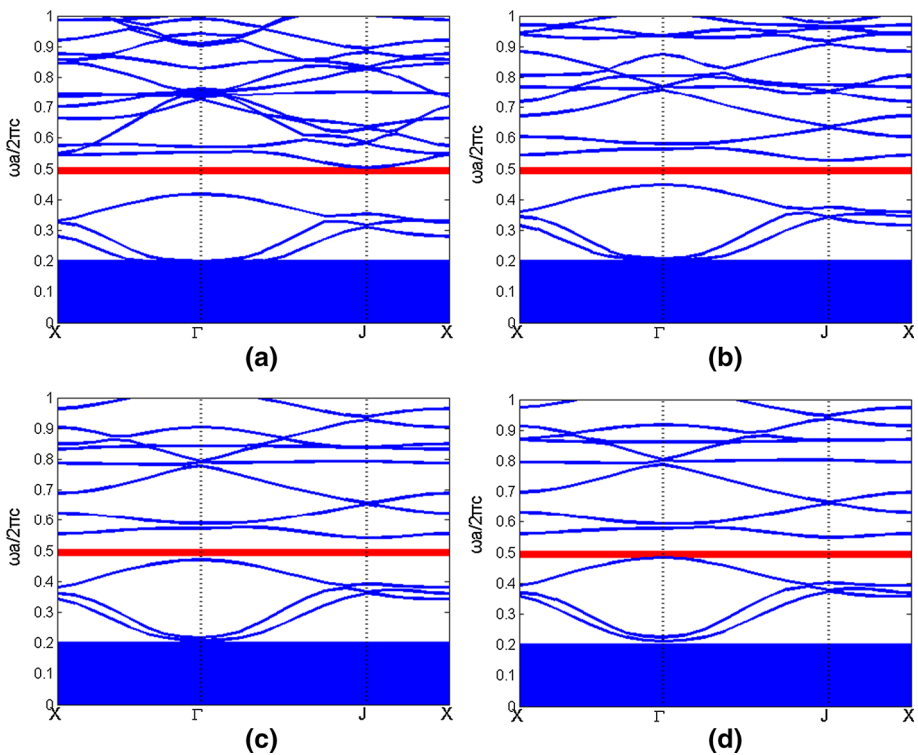


Fig. 2 The band structures for the proposed 2D PPCs with different incidence angle θ as $\varepsilon_a = 12.96$, $R = 0.46a$, $\omega_p = 0.2\omega_0$ and $v_c = 0.003\omega_p$. **a** $\theta = 0^\circ$, **b** $\theta = 45^\circ$, **c** $\theta = 66^\circ$ and **d** $\theta = 89^\circ$, respectively. The red shaded regions indicate the OBGs

existence of surface plasmon modes (Chern et al. 2006; Zhang et al. 2013b, 2015c), which are localized at the interface between the inserted plasma cylinders and the dielectric background. The similar phenomenon also can be observed in the 3D PPCs (Zhang et al. 2013b) or the PCs with metal (Chern et al. 2006) constituents. One also can see from Fig. 2a–d) the CPBGs of PPCs are located at $0.4174\text{--}0.5038$ ($2\pi c/a$), $0.4476\text{--}0.5264$ ($2\pi c/a$), $0.4707\text{--}0.5416$ ($2\pi c/a$) and $0.483\text{--}0.55492$ ($2\pi c/a$) as $\theta = 0^\circ$, 45° , 66° and 89° , respectively. From those results in Fig. 2, the OBG for proposed PPCs can be achieved. Obviously, the band edges of OBG can be determined by the upper edge of CPBG for $\theta = 0^\circ$ and the lower edge of CPBG for $\theta = 89^\circ$. In order to investigate the properties of OBG in the proposed 2D PPCs, the band structures are plotted in Fig. 3a as the values of ω_p are different. We can see from Fig. 3a that if $\omega_p = 0$, the plasma cylinders can be looked as the air cylinders. With increasing the incident angle θ , the band edges of CPBG are increased in the higher frequency regions, and the OBG (the area between two black dash lines) also can be obtained, which runs from 0.4753 to 0.4881 ($2\pi c/a$). If the plasma is introduced into such PCs ($\omega_p = 0.2\omega_0$), the edges of CPBGs will shift to higher frequency regions, whose OBG (the area between two green dash lines) spans 0.4830 to 0.5038 ($2\pi c/a$). Compared the results in Fig. 3a, the OBG is enlarged, whose bandwidth is increased to 0.008 ($2\pi c/a$) as the plasma is introduced into the conventional dielectric-air PCs. To further study, in Fig. 3b, we present band structures for such PPCs with similar case to Fig. 2 except that the ε_a is different. As shown in Fig. 3b, if the insert rods are air and $\varepsilon_a = 11.56$, there are not OBG and the CPBG will be closed at $\theta = 81^\circ$. If the air cylinders are replaced by the plasma ones, the OBG can be observed, which is located at $0.5157\text{--}0.5215$ ($2\pi c/a$). As mentioned above, compared to the conventional dielectric-air PCs, not only the OBG can be easier obtained in the PPCs but also the frequency range of OBG can be enhanced. Thus, the OBG can be obtained in the proposed PPCs.

In Fig. 4, the effects of R on the CPBGs and the relative bandwidth of OBG for the proposed 2D PPCs with $\varepsilon_a = 12.96$, $\omega_p = 0.2\omega_0$ and $v_c = 0.003\omega_p$ as $\theta = 0^\circ$ and $\theta = 89^\circ$. The shaded region indicates the OBG. As shown in Fig. 4a, both edges of CPBGs for $\theta = 0^\circ$ and 89° will shift to higher frequency regions, and their bandwidths will be increased first and then decreased as the value of R/a is increased. The lower edge of OBG is determined by the lower edge of CPBG for $\theta = 89^\circ$, and its upper edge is dependent on

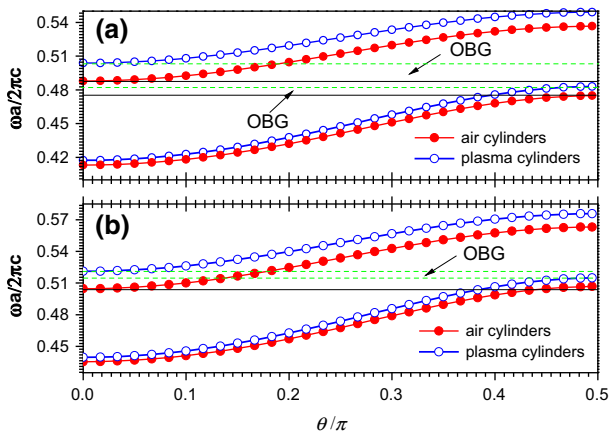


Fig. 3 The band structures for the two cases with similar case to Fig. 2 except that the ε_a are different. **a** $\varepsilon_a = 12.96$, and **(b)** $\varepsilon_a = 11.56$, respectively

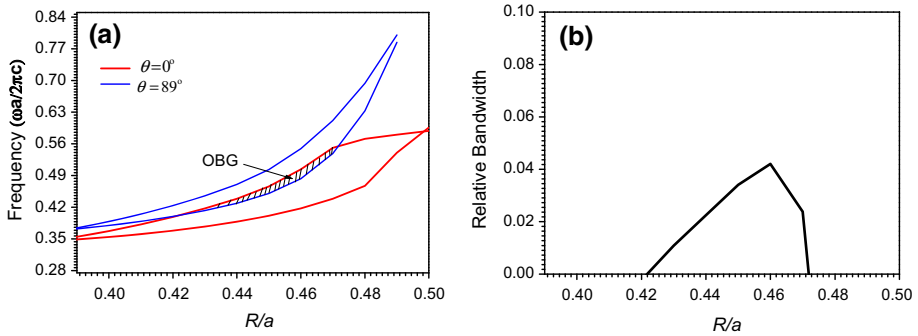


Fig. 4 The effects of R on the CPBGs and the relative bandwidth of OBG for the proposed 2D PPCs with $\epsilon_a = 12.96$, $\omega_p = 0.2\omega_0$, and $v_c = 0.003\omega_p$ as $\theta = 0^\circ$ and $\theta = 89^\circ$. **a** The CPBGs for the proposed 2D PPCs with different θ , and **(b)** the relative bandwidth of OBG

the upper of CPBG for $\theta = 0^\circ$. If $R/a < 0.42$ or $R/a > 0.47$, the OBG cannot be found. Compared to the CPBGs, the similar trends for the edges of OBG also can be seen in Fig. 4. In other words, the relative bandwidth of OBG also will be increased first and then decreased with the increasing value of R/a . As shown in Fig. 4b, the relative bandwidth of OBG will increase first and then decrease with the increasing value of R/a . The maximum bandwidth and relative bandwidth of OBG are $0.0208 (2\pi c/a)$ and 0.0421 , which can be observed at the case of $R/a = 0.46$, respectively. Compared to the case of $R/a = 0.47$, the frequency range and relative bandwidth of OBG are increased to $0.0078 (2\pi c/a)$ and 0.0183 , respectively. As mentioned above, we can choose a optimal value of R to obtain a larger OBG. Thus, R can be acted as an important parameter to manipulate the OBG, and the larger OBG can be observed in the high- R region.

In Fig. 5, we plot the effects of ω_p on the CPBGs and relative bandwidth of OBG for the proposed 2D PPCs with $\epsilon_a = 12.96$, $R = 0.46a$ and $v_c = 0.003\omega_p$ as $\theta = 0^\circ$ and $\theta = 89^\circ$. One can see from Fig. 5a that the trends for both edges of CPBGs for $\theta = 0^\circ$ and 89° are similar to those in Fig. 4. With the increasing value of ω_p/ω_0 , the edges of two CPBGs will shift to higher frequency regions, and their bandwidths also increase first and then decrease, whose maximum values are 0.1099 and $0.0680 (2\pi c/a)$, which can be found at the cases of $\omega_p/\omega_0 = 0.39$ and 0.33 , respectively. Consequently, the edges of OBG also

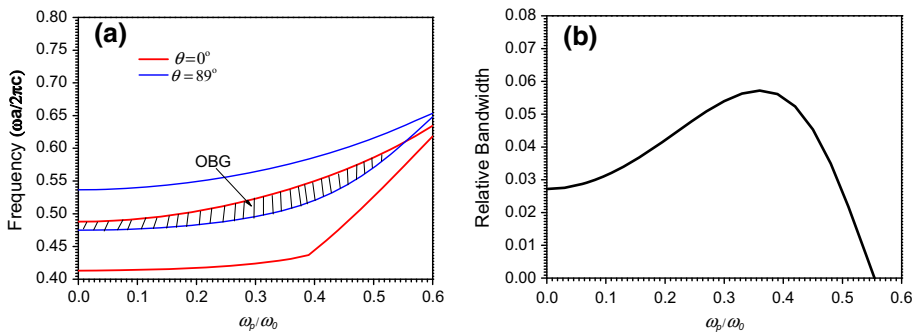


Fig. 5 The effects of ω_p on the CPBGs and the relative bandwidth of OBG for the proposed 2D PPCs with $\epsilon_a = 12.96$, $R = 0.46a$ and $v_c = 0.003\omega_p$ as $\theta = 0^\circ$ and $\theta = 89^\circ$. **a** The CPBGs for the proposed 2D PPCs with different θ , and **(b)** the relative bandwidth of OBG

will upward to the higher frequencies, and its bandwidth also increases first and then decreases as the value of ω_p/ω_0 is increased. It also can be seen from Fig. 5 that if $\omega_p/\omega_0 > 0.55$, the OBG will not exist. The largest OBG can be obtained at the case of $\omega_p/\omega_0 = 0.36$, whose frequency range is $0.02993 (2\pi c/a)$. In this case (as shown in Fig. 5b), the maximum relative bandwidth of OBG also can be observed, which is 0.0572. The trend of its relative bandwidth also increases first then decreases with increasing ω_p/ω_0 . Compared with the case of $\omega_p/\omega_0 = 0.21$, the frequency range and relative bandwidth of OBG are increased to $0.0085 (2\pi c/a)$ and 0.0138 , respectively. Increasing ω_p means that the real part of ε_p becomes smaller, and such effect is similar as increasing R . In other words, the averaged dielectric constant of present PPCs is changed (Joannopoulos et al. 1995). Thus, OBGs can be tuned and the larger OBG can be easily observed in the low- ω_p region. It is worth to be noticed that the OBG will not be enlarged with continuously the increasing value of ω_p .

3.2 Enhanced the OBGs by new PCs configurations

As we know, not only changing the parameters of PPCs can enlarge the OBG but also the OBG can be enhanced by breaking the symmetrical profiles of PPCs. In Fig. 6, schematic views of the two new PCs configurations are present. As shown in Fig. 6a, the 2D PPCs with triangular lattices are composed of two different sizes of plasma cylinders, whose radius are R_1 and R_2 . Obviously, if $R_1 = R_2$, the topology of PPCs will be same as those in Fig. 1 (the conventional structure). For convenience, such topological structure is named type-A structure. As shown in Fig. 6b, the other new configuration is that the rotated-square plasma rods are immersed into dielectric background with triangular lattices whose side length is d and filling factor is same as it in Fig. 1. In the other words, $d^2 = \pi R^2$. φ represents the angle between axes of the square cross section and the 2D lattices. In those cases, if the band structures are computed by the conventional PWE method, the equations for computing are complicated (Zhang et al. 2015c). Thus, the band structures can be calculated by a modified PWE method with mesh grid technique (Zhang et al. 2015c). The details of such technique can be seen in Ref. (Zhang et al. 2015c). In order to achieve a sufficiently high accuracy, the unit cell is meshed by 140×140 grids. In Fig. 7, the band structures of CPBGs for different PCs configurations as the incidence angle $\theta = 0^\circ$ are plotted. The red regions represents CPBGs. As shown in Fig. 7, there are two CPBGs for 2D PPCs with the conventional structure, which are located at $0.3657\text{--}0.3964 (2\pi c/a)$ and

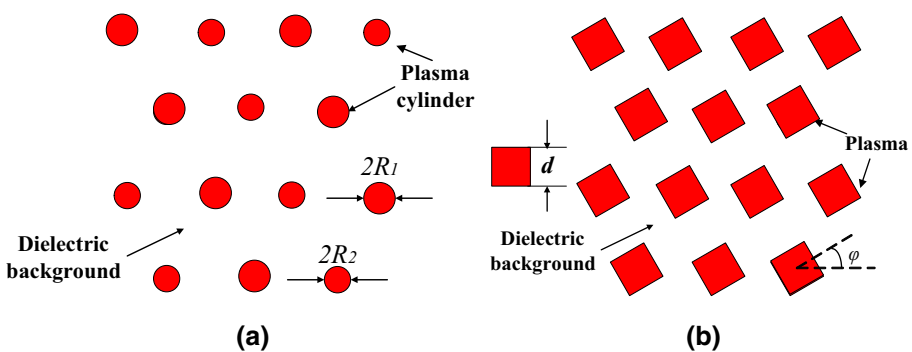


Fig. 6 Schematic views of two configurations of 2D PPCs to enhance the OBGs. **a** type-A structure, and **(b)** type-B structure

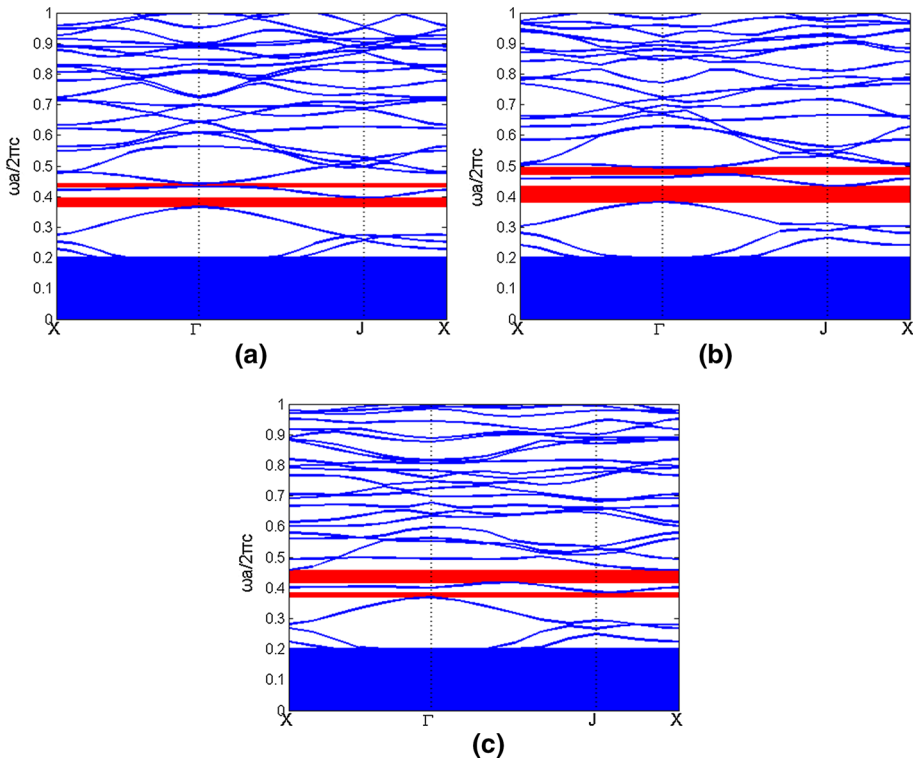


Fig. 7 The band structures of CPBGs for different PCs configurations as the incidence angle $\theta = 0^\circ$. **a** the 2D PPCs with similar case to Fig. 2 except for $R = 0.42a$, **(b)** the 2D PPCs with type-A structure as $R_1 = 0.42a$ and $R_2 = 0.47a$, and **(c)** the 2D PPCs with type-B structure with similar filling factor to **(a)** as $\varphi = 30^\circ$

0.4325–0.4419 ($2\pi c/a$). The parameters are the same as those in Fig. 2 except for $R = 0.42a$. If the 2D PPCs are with type-A structure as $R_1 = 0.42a$ and $R_2 = 0.47a$, those two CPBGs are covered 0.3825–0.4343 ($2\pi c/a$) and 0.4718–0.4948 ($2\pi c/a$). Similarly, the positions of such two CPBGs also will be changed to 0.3695–0.3847 ($2\pi c/a$) and 0.4208–0.4581 ($2\pi c/a$) as the 2D PPCs with type-B structure as $\varphi = 30^\circ$. Compared the results in Fig. 7, we can know that if the PPCs with type-A structure, the first (1st) CPBG can be enlarged, whose bandwidth is increased to 0.0211 ($2\pi c/a$). If the PPCs with type-B structure, the second (2nd) CPBG also can be enhanced, whose bandwidth is increased to 0.0279 ($2\pi c/a$). Thus, the CPBGs of PPCs for $\theta = 0^\circ$ can be enlarged by the two new PCs configurations.

According to the results in Fig. 7, the 1st OBG also may be enlarged as the PPCs with type-A structure, and the 2nd OBG may be enhanced as the PPCs with type-B structure. In order to prove this point, in Figs. 8 and 9, we plot the band edges of CPBGs a function of incident angle θ for the 2D PPCs with such two different configurations as $\varepsilon_a = 12.96$, $\omega_p = 0.2\omega_0$ and $\nu_c = 0.003\omega_p$. As shown in Fig. 8, if $R_1 = 0.47a$ and $R_2 = 0.46a$, the band edges of 1st CPBGs move to higher frequency regions as θ is increased, and there is an OBG (the area between two green dash lines) which runs from 0.4967 to 0.5188 ($2\pi c/a$). If $R_1 = R_2 = 0.46a$, the band edges of CPBGs move to higher frequency regions, and there is an OBG (the area between two black solid lines) which spans from 0.4830 to

Fig. 8 The band edges of 1st CPBGs a function of incident angle θ for the 2D PPCs with type-A structure as the R_1 are different

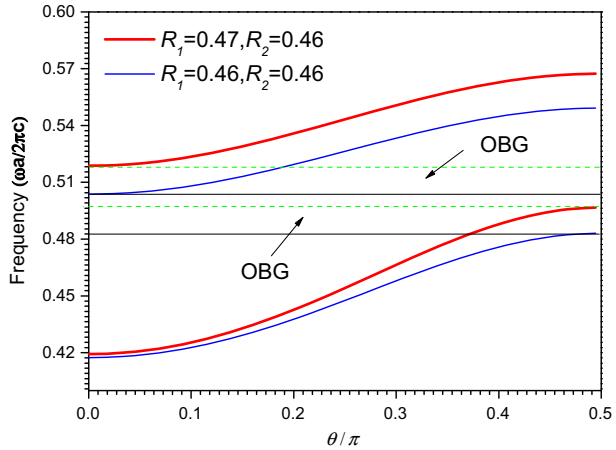
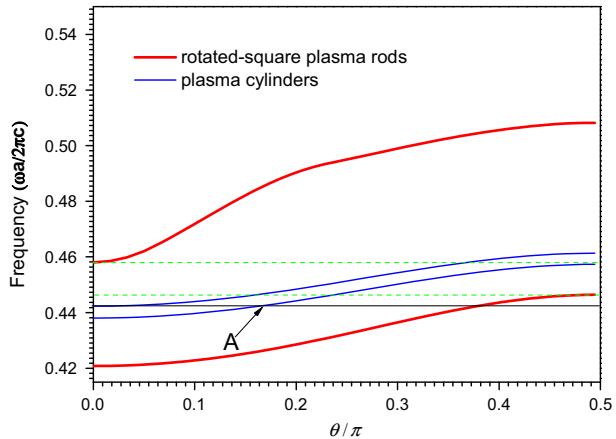


Fig. 9 The band edges of 2nd CPBGs a function of incident angle θ for the 2D PPCs with type-B structure as the filler are different and rotated angle $\varphi = 30^\circ$



0.5038 ($2\pi c/a$). Compared with the results in Fig. 8, the 1st OBG can be enlarged as the PPCs with type-A structure which is increased to 0.0013 ($2\pi c/a$). Similar phenomenon also can be observed in Fig. 9. The 2nd OBG can be obtained as the PPCs with type-B structure and $\varphi = 30^\circ$, which is located from 0.4465 to 0.4581 ($2\pi c/a$). However, for the conventional 2D PPCs, the 2nd OBG does not exist and the CPBG will be closed at $\theta = 31^\circ$ (A point in Fig. 9). In other words, upper and lower edges of the CPBG will coincide at point A. Compared with the 2nd OBG in the conventional case, the 2nd OBG for the PPCs with type-B structure is enhanced obviously, and its bandwidth is increased to 0.0116 ($2\pi c/a$). Thus, the OBGs can be widened as the PPCs with such two configurations. It means that we can enhance the different OBGs by the present PCs structures according to the practical needs.

In order to further study the effects of parameters for two new configurations on the properties of OBGs, we display the effects of R_1 on the CPBGs and the relative bandwidth of 1st OBG for the 2D PPCs with type-A structure and $\varepsilon_a = 12.96$, $R_2 = 0.46a$, $\omega_p = 0.2\omega_0$, $\nu_c = 0.003\omega_p$ as $\theta = 0^\circ$ and $\theta = 89^\circ$ in Fig. 10. The shaded region indicates the OBG. As shown in Fig. 10a, the band edges of 1st CPBGs for $\theta = 0^\circ$ and $\theta = 89^\circ$ shift

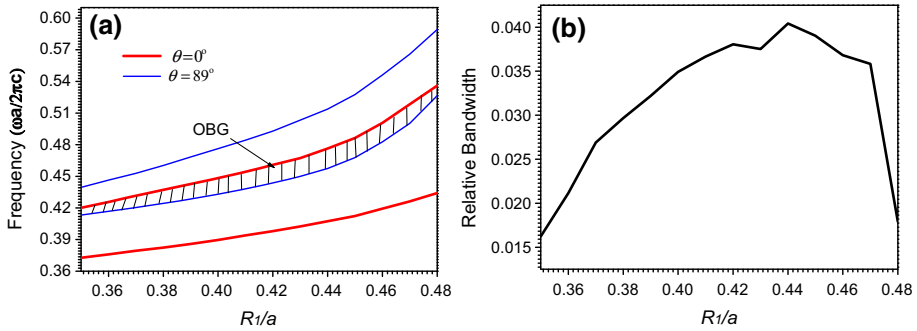


Fig. 10 The effects of R_1 on the CPBGs and the relative bandwidth of 1st OBG for the 2D PPCs with type-A structure and $\epsilon_a = 12.96$, $R_2 = 0.46a$, $\omega_p = 0.2\omega_0$, $v_c = 0.003\omega_p$ as $\theta = 0^\circ$ and $\theta = 89^\circ$. **a** The CPBGs for the proposed 2D PPCs with different θ , and **(b)** the relative bandwidth of 1st OBG

to higher frequency regions, and their bandwidths will increase with increasing the value of R_1/a . The similar trends for the edges of 1st OBG also can be observed but its bandwidth increases first and then decreases as the value of R_1/a is increased. The maximum bandwidth of 1st OBG is $0.01887 (2\pi c/a)$, which can be found at the case of $R_1/a = 0.44$. Compared with the results in Fig. 7a, the PPCs with type-A structure have the advantages of obtaining the larger 1st OBG, especially, in the low- R_1/a region. As shown in Fig. 10b, the trend of relative bandwidth will increase first and then decrease with increasing R_1 . The maximum value is 0.0404 at the case of $R_1/a = 0.44$. Compared with the case of $R_1/a = 0.46$, the relative bandwidth is increased to 0.0036.

In Fig. 11, we plot the effects of d on the CPBGs and the relative bandwidth of 2nd OBG for the 2D PPCs with type-B structure and $\epsilon_a = 12.96$, $\varphi = 30^\circ$, $\omega_p = 0.2\omega_0$, $v_c = 0.003\omega_p$ as $\theta = 0^\circ$ and $\theta = 89^\circ$. As shown in Fig. 11a, the both band edges of CPBGs for $\theta = 0^\circ$ and $\theta = 89^\circ$ will move to higher frequency regions, and their bandwidths will increase with the increasing value of d/a . The similar trends for the band edges of 2nd OBG also can be observed in Fig. 11a but its bandwidth will increase first and then decrease as d/a is increased. If $d/a < 0.676$ or $d/a > 0.78$, the OBG will disappear. Obviously, it can be seen from Fig. 11b that the relative bandwidth of 2nd OBG also will increase first and then decrease with increasing d . The maximum bandwidth and relative

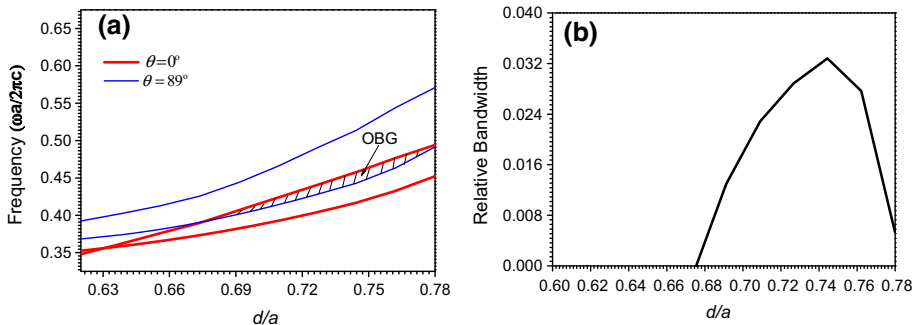


Fig. 11 The effects of d on the 2nd CPBGs and the relative bandwidth of 2nd OBG for the 2D PPCs with type-B structure and $\epsilon_a = 12.96$, $\varphi = 30^\circ$, $\omega_p = 0.2\omega_0$, $v_c = 0.003\omega_p$ as $\theta = 0^\circ$ and $\theta = 89^\circ$. **a** The CPBGs for the proposed 2D PPCs with different θ , and **(b)** the relative bandwidth of 2nd OBG

bandwidth of OBG are 0.01478 ($2\pi c/a$) and 0.03282, which can be observed at the case of $d/a = 0.744$, respectively. Compared with the case of $d/a = 0.7$, the frequency range and relative bandwidth of 2nd OBG are increased to 0.01 ($2\pi c/a$) and 0.0198, respectively. Thus, the PPCs with type-B structure can improve the properties of 2nd OBG, and the larger 2nd OBG also can be obtained in the high- d region. It means that the 2nd OBG can be manipulated by choosing a suitable value of d .

In Fig. 12, we plot the effects of φ on the CPBGs and the relative bandwidth of 2nd OBG for the 2D PPCs with type-B structure and $\epsilon_a = 12.96$, $d = 0.744a$, $\omega_p = 0.2\omega_0$, $\nu_c = 0.003\omega_p$ as $\theta = 0^\circ$ and $\theta = 89^\circ$. It can be seen from Fig. 12a that if $\varphi \geq 23^\circ$ and $\varphi \leq 64^\circ$, the 2nd OBG for proposed PPCs can be observed. The upper edge of OBG move to lower frequencies first and then shift higher frequency regions with increasing φ , but the trend for lower edge of OBG is irregular as the value of φ is changed. If the rotated angle of inserted square plasma rods are 23° , 42° and 64° , such OBG hardly can be observed. As shown in Fig. 12b, if $\varphi = 54^\circ$, the maximum bandwidth and relative bandwidth of such OBG can be obtained, which are 0.04061 ($2\pi c/a$) and 0.09074, respectively. According to the results in Fig. 12a, we can know that there is an optimal value of φ to achieve the largest frequency range of 2nd OBG for the PPCs with type-B structure as the filling factor is never changed. In other words, the OBG can be enlarged and manipulated by changing φ . This can be explained that changing φ means the symmetrical profile of PPCs is broken. Thus, φ is an important parameter which is needed to be chosen. Of course, the OBG also can be enhanced and tuned by introducing the anisotropic dielectric into PPCs as mentioned in Ref. (Li et al. 1999). We will study this in next part.

In order to investigate the effects anisotropic dielectric background on the OBG, in Fig. 13, the band structures of CPBGs for different dielectric background as the incidence angle $\theta = 0^\circ$ are plotted. Obviously, the proposed cases are with similar case to Fig. 2 except for $R = 0.47a$ or the dielectric background is different. As we know, the expression for the conventional dielectric can be written as

$$\epsilon_a = \begin{pmatrix} \epsilon_{xx} & 0 & 0 \\ 0 & \epsilon_{yy} & 0 \\ 0 & 0 & \epsilon_{zz} \end{pmatrix} \tag{2}$$

where $\epsilon_{xx} = n_x^2$, $\epsilon_{yy} = n_y^2$, $\epsilon_{zz} = n_z^2$. If $\epsilon_{xx} = \epsilon_{yy} = \epsilon_{zz}$, the conventional isotropic dielectric can be obtained. If the value of ϵ_{xx} is not equal to that for ϵ_{yy} or ϵ_{zz} , the anisotropic dielectric

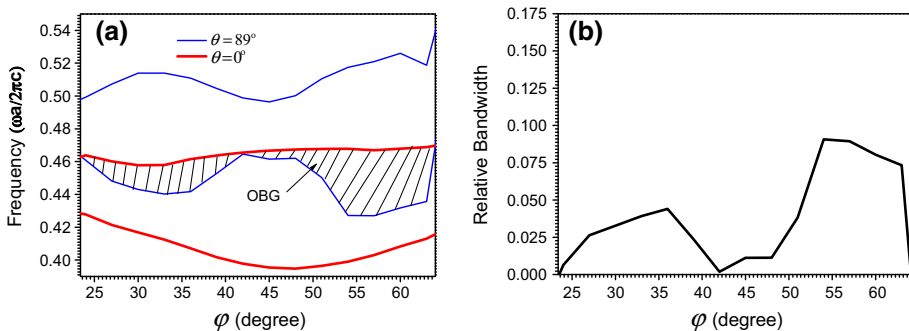


Fig. 12 The effects of φ on the CPBGs and the relative bandwidth of 2nd OBG for the 2D PPCs with type-B structure and $\epsilon_a = 12.96$, $d = 0.744a$, $\omega_p = 0.2\omega_0$, $\nu_c = 0.003\omega_p$ as $\theta = 0^\circ$ and $\theta = 89^\circ$. **a** The CPBGs for the proposed 2D PPCs with different θ , and **(b)** the relative bandwidth of 2nd OBG

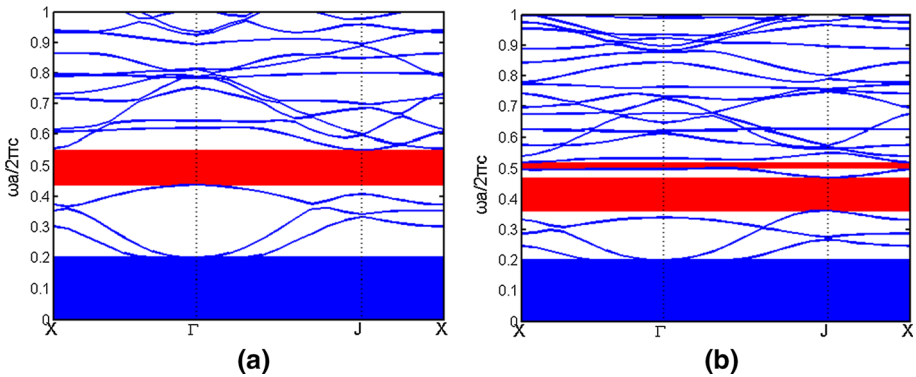


Fig. 13 The band structures of CPBGs for different dielectric background as the incidence angle $\theta = 0^\circ$. **a** the 2D PPCs with similar case to Fig. 2 except for $R = 0.47a$, **(b)** the 2D PPCs with similar case to Fig. 2 except for $R = 0.47a$ and dielectric background is anisotropic. The red regions present the CPBGs

can be achieved. In the nature, the anisotropic dielectric can be found easily. The typical anisotropic dielectric is the uniaxial material, such as Te and Ti_3AsSe_3 (Li et al. 1999). For the uniaxial material, two different principal-refractive indices can be obtained, which are named ordinary-refractive and extraordinary-refractive indices (n_o and n_e), respectively. In Fig. 13b, we only consider a simpler case, which is that the extraordinary axis of anisotropic dielectric background (uniaxial material) is parallel to the inserted plasma cylinders ($\epsilon_{xx} = n_o^2 = 4.8^2$, $\epsilon_{yy} = \epsilon_{zz} = n_e^2 = 6.2^2$). As shown in Fig. 13a, for the conventional isotropic dielectric background ($\epsilon_{xx} = \epsilon_{yy} = \epsilon_{zz} = 12.96$), there is one CPBG can be found as the incidence angle $\theta = 0^\circ$, which runs from 0.4346 to 0.5436 ($2\pi c/a$). The frequency range of CPBG is 0.109 ($2\pi c/a$). As a comparison, we can see from Fig. 13b that there exist two CPBGs, which are covered 0.3539–0.4648 ($2\pi c/a$) and 0.4907–0.5207 ($2\pi c/a$), respectively. The bandwidths are 0.1109 and 0.03 ($2\pi c/a$), respectively. Compared with the results in Fig. 13a, b, we can know that not only the bandwidth of CPBG can be enhanced but also the number of CPBG is increased by introducing the anisotropic dielectric (uniaxial material) into the proposed 2D PPCs. In order to further study the effects anisotropic dielectric background on the OBG, in Fig. 14, we display the band edges of CPBGs a function of incident angle θ for the 2D PPCs with the different dielectric background as

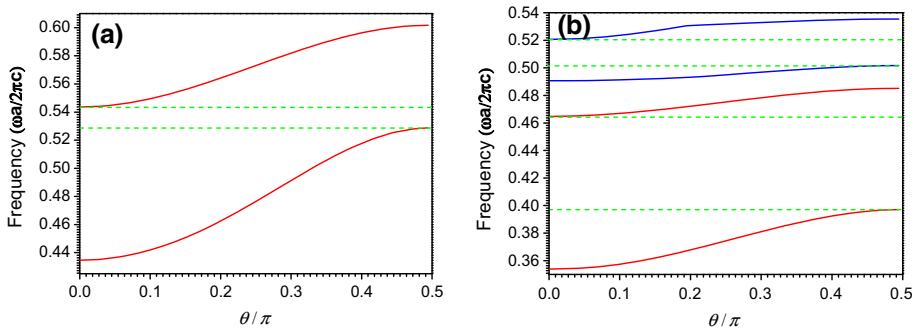


Fig. 14 The band edges of 1st CPBGs a function of incident angle θ for the 2D PPCs with different dielectric background. **a** the dielectric background is the conventional isotropic dielectric ($\epsilon_a = 12.96$), **(b)** the dielectric background is anisotropic dielectric

$R = 0.47a$, $\omega_p = 0.2\omega_0$ and $v_c = 0.003\omega_p$. The regions between the green dash lines are OBGs. As shown in Fig. 14a, the edges of CPBGs move to higher frequency region with increasing the incident angle θ . There is a OBG, which spans from 0.5288 to 0.5436 ($2\pi c/a$). The bandwidth of such OBG is 0.0148 ($2\pi c/a$). We also can see from Fig. 14b that the edges of two CPBGs for the proposed 2D PPCs with the anisotropic dielectric background shift to higher frequency region, and two OBGs can be observed. Those two OBGs are located 0.3972–0.4648 ($2\pi c/a$) and 0.5016–0.5207 ($2\pi c/a$), whose bandwidths are 0.0676 and 0.0191 ($2\pi c/a$), respectively. Compared with the results in Fig. 14, we can know that not only the OBG also can be enlarged but also the number of OBG also can be increased, when the conventional isotropic dielectric background is changed to the anisotropic dielectric. Thus, the OBG of proposed 2D PPCs can be enhanced by introducing the anisotropic dielectric.

In Fig. 15, we plot the effects of n_o on the CPBGs and the relative bandwidth of 1st OBG for the 2D PPCs with the anisotropic dielectric background ($\epsilon_{xx} = n_o^2, \epsilon_{yy} = \epsilon_{zz} = n_e^2$) and $n_e = 6.2$, $R = 0.47a$, $\omega_p = 0.2\omega_0$, and $v_c = 0.003\omega_p$ as $\theta = 0^\circ$ and $\theta = 89^\circ$. The shaded region indicates the OBG. As shown in Fig. 15a, the both band edges of CPBGs for $\theta = 0^\circ$ and $\theta = 89^\circ$ will shift to lower frequency regions, and their bandwidths will increase first and then decrease with the increasing value of n_o . The similar trends for the band edges of 1st OBG also can be obtained in Fig. 15a. If $n_o < 3.3$, the 1st OBG cannot be observed. Obviously, the maximum bandwidth of 1st OBG can be found at the case of $n_o = 4.8$, which is 0.0676 ($2\pi c/a$). It also can be seen from Fig. 15b that the relative bandwidth of 1st OBG also will increase first and then decrease with increasing n_o . The maximum relative bandwidth of such OBG is 0.1535, which can be observed at the case of $n_o = 4.8$. Compared with the case of $n_o = 5.6$, the bandwidth and relative bandwidth of 1st OBG are increased to 0.0187 ($2\pi c/a$) and 0.0334, respectively. Thus, the properties of 1st OBG for the 2D PPCs can be manipulated obviously by changing the value of n_o , and the larger 1st OBG also can be obtained in the mid- n_o region.

In Fig. 16, we present the effects of n_e on the CPBGs and the relative bandwidth of 1st OBG for the 2D PPCs with the anisotropic dielectric background and $n_o = 4.8$, $R = 0.47a$, $\omega_p = 0.2\omega_0$, and $v_c = 0.003\omega_p$ as $\theta = 0^\circ$ and $\theta = 89^\circ$. The shaded region indicates the OBG. It can be seen from Fig. 12a that the band edges of 1st CPBG for $\theta = 0^\circ$ hardly varies with changing the value of n_e but the band edges of 1st CPBG for $\theta = 89^\circ$ shift to lower frequency region slightly. Obviously, the frequency range of 1st CPBGs for $\theta = 0^\circ$

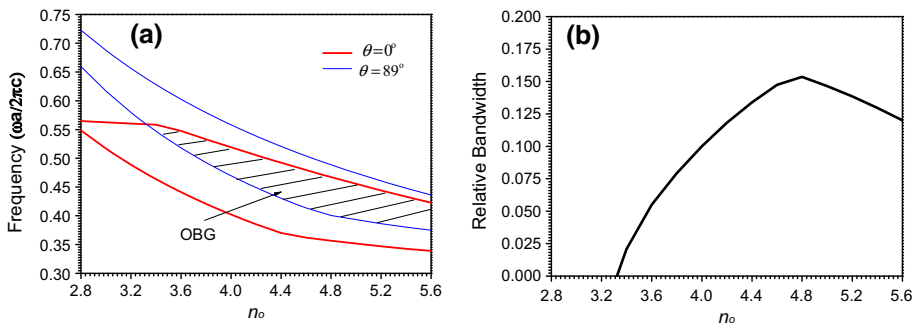


Fig. 15 The effects of n_o on the CPBGs and the relative bandwidth of 1st OBG for the proposed 2D PPCs with $n_e = 6.2$, $R = 0.47a$, $\omega_p = 0.2\omega_0$, and $v_c = 0.003\omega_p$ as $\theta = 0^\circ$ and $\theta = 89^\circ$. **a** The CPBGs for the proposed 2D PPCs with different θ , and **(b)** the relative bandwidth of 1st OBG

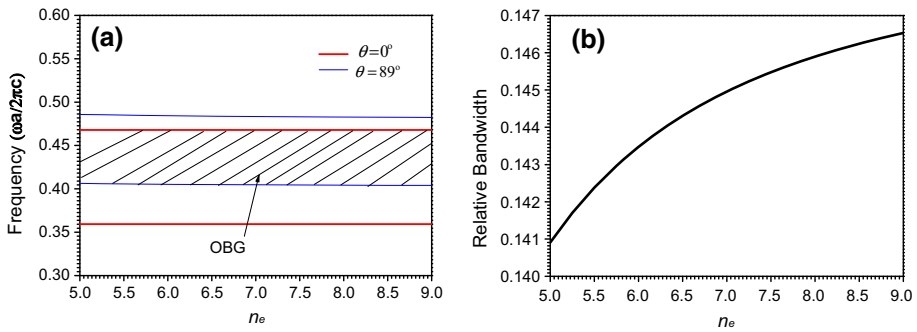


Fig. 16 The effects of n_e on the CPBGs and the relative bandwidth of 1st OBG for the proposed 2D PPCs with $n_o = 4.8$, $R = 0.47a$, $\omega_p = 0.2\omega_0$, and $v_c = 0.003\omega_p$ as $\theta = 0^\circ$ and $\theta = 89^\circ$. **a** The CPBGs for the proposed 2D PPCs with different θ , and **(b)** the relative bandwidth of 1st OBG

is almost unchanged but that for $\theta = 89^\circ$ is decreased with the increasing value of n_e . The trends for the edges of 1st OBG also can be observed from Fig. 16a, the upper edge of 1st OBG is almost unchanged but it's the lower edge shift to lower frequency region slightly. Thus, the bandwidth of 1st OBG will be enhanced with increasing the increasing value of n_e . The maximum bandwidth of 1st OBG can be observed at the case of $n_e = 9$, which is $0.0639 (2\pi c/a)$. As shown in Fig. 16b, the trend of relative bandwidth will increase with the increasing value of n_e . The maximum value is 0.1465 at the case of $n_e = 9$. Thus, maximum bandwidth and relative bandwidth of 1st OBG can be founded at the case of $n_e = 9$. Compared to the case of $n_e = 5$, those values are increased to $0.0023 (2\pi c/a)$ and 0.0056, respectively. It can be seen from the results in Fig. 16 that the 1st OBG cannot be manipulated by changing the increasing value of n_e in a large frequency range. The bandwidth of 1st OBG only can be enlarged slightly by increasing n_e . As mentioned above, the 1st OBG can be tuned slightly by changing n_e , and the larger 1st OBG can be achieved in the high- n_e region. According to the results in Figs. 15 and 16, in our case, the 1st OBG for the proposed PPCs can be tuned in a larger frequency region by changing n_o compared with tuning n_e .

It is worth to be noticed that the plasma cylinders/square rods can be realized, which are mentioned in this paper. In order to obtain the plasma cylinders/square rods, we can use the Helium as a working gas to generate the plasmas material, (obviously, the tubes with double-shell structures), and the plasma cylinders or square rods with double-shell structures are ionized by the direct current. The plasma cylinders/square can be realized by the the commercial quartz discharge tubes, which are argon-filled to a pressure of 550 Pa with added mercury (to obtain the larger plasma frequency). The details of this part will be proposed in another paper.

4 Conclusions

In summary, the features of CPBGs and OBGs in the 2D PPCs with triangular lattices are theoretically investigated in detail by the PWE method as the incidence wave is off-plane, which are containing the non-magnetized plasma cylinders inserted into the homogeneous and isotropic dielectric background. According to the theoretical simulation results, some conclusions can be obtained. If the plasma is introduced into 2D dielectric PCs, not only

tunable OBGs can be obtained but also a flatbands region can be observed since existing the surface plasmon modes, whose frequency range is less than ω_p . In such region, the group velocity of EM wave is every low. Compared to the conventional 2D dielectric-air PCs, the OBG is easier achieved and the larger OBG also can be observed in the 2D PPCs with same structure. In other words, the 2D PPCs are more suitable than the conventional 2D dielectric-air PCs to realize the omnidirectional reflector or mirror. The effects of R and ω_p on the properties of OBG also are studied in calculation, respectively. The calculated results demonstrated that the OBG can be manipulated obviously by changing R and ω_p . Increasing R and ω_p , the band edges of CPBGs and OBG shift to higher frequency regions, and their bandwidths and relative bandwidths will increase first and then decrease, whose maximum values can be found in the high- R and low- ω_p regions. As a comparison, two new configurations of 2D PPCs also are proposed to enlarge the OBGs since the symmetrical profile of PPCs is broken. The simulated results reveal that the 1st OBG can be enhanced as the PPCs with type-A structure, and the 2nd OBG can be broadened as the PPCs with type-B structure. For type-A structure, if R_2 remains a constant and unchanged, the larger 1st OBG can be observed in the high- R_1 region compared to the conventional 2D PPCs. For type-B structure, the 2nd OBG can be enhanced obviously in the high- d and high- φ regions. Compared to changing d , the OBG is more sensitive to the value of φ . However, it is worth to be noticed that the two newly proposed configurations cannot help to enhance all of OBGs in the conventional PPCs, and we have to choose the optimizations according to the practical applications. Introducing the anisotropic dielectric (uniaxial material) into the proposed 2D PPCs to enlarge the OBG also is studied. The effects of n_o and n_e of uniaxial material on the properties of OBG also are investigated in theory, respectively. The computed results shown that the OBG can be manipulated obviously by changing n_o but it will be tuned slightly by changing n_e . Compared with changing n_e , the OBG can be tuned in a larger frequency region by changing n_o . The larger 1st OBG can be obtained in the mid- n_o or high- n_e regions. As mentioned above, those theoretical results may open a new scope to design the omnidirectional reflector or mirror based on the 2D PPCs.

Acknowledgements This work was supported by the National Natural Science Foundation of China (Grant No. 61307052) and Chinese Jiangsu Planned Projects for Postdoctoral Research Funds (Grant No. 1501016A), and Project Funded by China Postdoctoral Science Foundation (Grant No. 2015M581790), and the special grade of the financial support from the China Postdoctoral Science Foundation (Grant No. 2016T90455).

References

- Aly, A.H., Elsayed, H.A., El-Naggar, S.A.: The properties of cutoff frequency in two-dimensional superconductor photonic crystals. *J. Mod. Opt.* **61**, 1064–1068 (2014)
- Ardakani, A.G.: Nonreciprocal electromagnetic wave propagation in one-dimensional ternary magnetized plasma photonic crystals. *J. Opt. Soc. Am. B* **31**, 332–339 (2014)
- Biancalana, F.: All-optical diode action with quasiperiodic photonic crystals. *J. Appl. Phys.* **104**, 093113 (2008)
- Chern, R.L., Chang, C.C., Chang, C.C.: Analysis of surface plasmon modes and band structures for plasmonic crystals in one and two dimensions. *Phys. Rev. E* **73**, 036605 (2006)
- Feng, X.P., Arakawa, Y.: Off-plane angle dependence of photonic band gap in a two-dimensional photonic crystal. *IEEE J. Quantum Electron.* **32**, 535–542 (1996)
- Fu, T., Yang, Z., Shi, Z., Lan, F., Li, D., Gao, X.: Dispersion properties of a 2D magnetized plasma metallic photonic crystal. *Phys. Plasmas* **20**, 023109 (2013)
- Ginzburg, V.L.: *The Propagation of Electromagnetic Wave in Plasma*. Pergamon, Oxford (1970)

- Haas, T., Hesse, A., Doll, T.: Omnidirectional two-dimensional photonic crystal band gap structures. *Phys. Rev. B* **73**, 045130 (2006)
- Hamidi, S.M.: Optical and magneto-optical properties of onedimensional magnetized coupled resonator plasma photonic crystals. *Phys. Plasmas* **19**, 012503 (2012)
- Hart, S.D., Maskaly, G.R., Temelkuran, B., Prideaux, P.H., Joannopoulos, J.D., Fink, Y.: External reflection from omnidirectional dielectric mirror fibers. *Science* **296**, 510–513 (2002)
- Hojó, H., Mase, A.: Dispersion relation of electromagnetic waves in one dimensional plasma photonic crystals. *Plasma Fusion Res.* **80**, 89–90 (2004)
- Joannopoulos, J.J., Meade, R.D., Winn, J.N.: *Photonic Crystals: Molding the Flow of Light*. Princeton University Press, New Jersey (1995)
- John, S.: Strong localization of photons in certain disordered dielectric superlattices. *Phys. Rev. Lett.* **58**, 2486–2489 (1987)
- King, T., Kuo, W., Yang, T., Bian, T., Wu, C.: Magnetic-field dependence of effective plasma frequency for a plasma photonic crystal. *IEEE Photon. J.* **5**, 4700110 (2013)
- Kuzmiak, V., Maradudin, A.A.: Photonic band structure of one-and two-dimensional periodic systems with metallic components in the presence of dissipation. *Phys. Rev. B* **55**, 7427–7444 (1997)
- Li, Z.Y., Xia, Y.: Omnidirectional absolute band gaps in two-dimensional photonic crystals. *Phys. Rev. B* **64**, 153108 (2001)
- Li, Z., Gu, B., Yang, G.: Improvement of absolute band gaps in 2D photonic crystals by anisotropy in dielectricity. *Eur. Phys. J. B* **11**, 65–73 (1999)
- Li, C.Z., Liu, S.B., Kong, X.K., Zhang, H.F., Bian, B.R., Zhang, X.Y.: A novel comb-like plasma photonic crystal filter in the presence of evanescent wave. *IEEE Trans. Plasma Sci.* **39**, 1969–1973 (2011)
- Mekis, A., Chen, J.C., Kurland, I., Fan, S., Villeneuve, P.R., Joannopoulos, J.J.: High transmission through sharp bends in photonic crystals waveguide. *Phys. Rev. Lett.* **77**, 3787–3790 (1996)
- Qi, L.: Photonic band structures of two-dimensional magnetized plasma photonic crystals. *J. Appl. Phys.* **111**, 073301 (2012)
- Qi, L., Zhang, X.: Band gap characteristics of plasma with periodically varying external magnetic field. *Solid State Commun.* **151**, 1838–1841 (2011)
- Russell, P.: Photonic crystals fibers. *Science* **299**, 358–362 (2003)
- Sakai, O., Tachibana, K.: Plasma as metamaterial: a review. *Plasma Sources Sci. Technol.* **21**, 013001 (2012)
- Sakoda, K.: *Optical Properties of Photonic Crystals*. Springer, Berlin (2001)
- Shiverhwari, L.: Zero permittivity band characteristics in one dimensional plasma dielectric photonic crystal. *Opt.-Int. J. Light Electron. Opt.* **122**, 1523–1526 (2011)
- Shukla, S., Prasad, S., Singh, V.: Properties of surface modes in one dimensional plasma photonic crystals. *Phys. Plasmas* **22**, 022122 (2015)
- Sözüer, H., Haus, J., Inguva, R.: Photonic bands: convergence problems with the plane-wave method. *Phys. Rev. B* **45**, 13962 (1992)
- Tian, H., Zi, J.: One-dimensional tunable photonic crystals by means of external magnetic field. *Opt. Commun.* **252**, 321–328 (2005)
- Winn, J.N., Fink, Y., Fan, S., Joannopoulos, J.D.: Omnidirectional reflection from a one-dimensional photonic crystals. *Opt. Lett.* **23**, 1573–1575 (1998)
- Xiang, Y., Dai, X., Wen, S., Dan, F.: Omnidirectional and multiple-channeled high-quality filters of photonic heterostructures containing single-negative materials. *J. Opt. Soc. Am. A* **23**, A28–A32 (2007)
- Yablonovitch, E.: Inhibited spontaneous emission of photons in solidstate physics and electronics. *Phys. Rev. Lett.* **58**, 2059–2061 (1987)
- Zhang, H.F., Liu, S.B.: Study on the properties of switching bandgap and surface plasmon modes in 3-D plasma photonic crystals with pyrochlore lattices in core-shell structure. *IEEE Trans. Plasma Sci.* **42**, 1839–1846 (2014)
- Zhang, H.F., Liu, S.B., Kong, X.K., Zou, L., Li, C.Z., Qing, W.S.: Enhancement of omnidirectional photonic band gaps in one-dimensional dielectric plasma photonic crystals with a matching layer. *Phys. Plasmas* **19**, 022103 (2012a)
- Zhang, H.F., Liu, S.B., Kong, X.K., Bian, B.R., Dai, Y.: Omnidirectional photonic band gap enlarged by one-dimensional ternary unmagnetized plasma photonic crystals based on a new Fibonacci quasiperiodic structure. *Phys. Plasmas* **19**, 112102 (2012b)
- Zhang, H.F., Liu, S.B., Kong, X.K., Zhou, L., Li, C.Z., Bian, B.R.: Enlarged omnidirectional photonic band gap in heterostructure of plasma and dielectric photonic crystals. *Opt.-Int. J. Light Electron. Opt.* **124**, 751–756 (2013a)

- Zhang, H.F., Liu, S.B., Kong, X.K., Chen, C., Bian, B.R.: The characteristics of photonic band gaps for three-dimensional unmagnetized dielectric plasma photonic crystals with simple-cubic lattice. *Opt. Commun.* **288**, 82–90 (2013b)
- Zhang, H.F., Liu, S.B., Jiang, C.J.: The properties of photonic band gap and surface plasmon modes in the three-dimensional magnetized plasma photonic crystals as the mixed polarized modes considered. *J. Plasma Phys.* **81**, 905810201 (2015a)
- Zhang, H.F., Liu, S.B., Li, B.X., Chen, C.Q.: Analyzing the properties of acceptor mode in two-dimensional plasma photonic crystals based on a modified finite-difference frequency-domain method. *Phys. Plasmas* **22**, 112103 (2015b)
- Zhang, H.-F., Ding, G.-W., Li, H.-M., Liu, S.-B.: Complete photonic band gaps and tunable self-collimation in the two-dimensional plasma photonic crystals with a new structure. *Phys. Plasmas* **22**, 022105 (2015c)
- Zhang, H.F., Liu, S.B., Li, B.X.: Investigation on the properties of omnidirectional photonic band gaps in two-dimensional plasma photonic crystals. *Phys. Plasmas* **23**, 012105 (2016)